Ion density of positive and negative ions at ambient pressure in air at 12-136 mm from 4.9 kV soft x-ray source

Anttalainen, Osmo

2021-05-01

Anttalainen , O , Lattouf , E , Kotiaho , T & Eiceman , G 2021 , ' Ion density of positive and negative ions at ambient pressure in air at 12-136 mm from 4.9 kV soft x-ray source ' , Review of Scientific Instruments , vol. 92 , no. 5 , 054104 . https://doi.org/10.1063/5.0050669

http://hdl.handle.net/10138/334396
https://doi.org/10.1063/5.0050669

Review of Scientific Instruments

Ion density of positive and negative ions at ambient pressure in air at 12–136 mm from 4.9 kV soft x-ray source

Cite as: Rev. Sci. Instrum. **92**, 054104 (2021); https://doi.org/10.1063/5.0050669
Submitted: 17 March 2021 . Accepted: 24 April 2021 . Published Online: 10 May 2021

Osmo Anttalainen, Elie Lattouf, Tapio Kotiaho, Gary Eiceman, et al.

AIP Publishing

Ion density of positive and negative ions at ambient pressure in air at 12–136 mm from 4.9 kV soft x-ray source

Cite as: Rev. Sci. Instrum. 92, 054104 (2021); doi: 10.1063/5.0050669
Submitted: 17 March 2021 • Accepted: 24 April 2021 •
Published Online: 10 May 2021

Osmo Anttalainen,[1,a] Elie Lattouf,[1] Tapio Kotiaho,[2,3] and Gary Eiceman[1,4]

AFFILIATIONS

[1] VERIFIN, Finnish Institute for Verification of the Chemical Weapons Convention, Department of Chemistry, University of Helsinki, FI-00014 Helsinki, Finland
[2] Drug Research Program and Division of Pharmaceutical Chemistry and Technology, Faculty of Pharmacy, University of Helsinki, P.O. Box 56, FI-00014 Helsinki, Finland
[3] Department of Chemistry, Faculty of Science, University of Helsinki, P.O. Box 55, FIN-00014 Helsinki, Finland
[4] Department of Chemistry and Biochemistry, New Mexico State University, 1175 N. Horseshoe Dr., Las Cruces, New Mexico 88003, USA

[a] **Author to whom correspondence should be addressed:** osmo.anttalainen@helsinki.fi

ABSTRACT

The abundance of ions is an essential parameter for ion mobility and mass spectrometry instrument design and for the control or optimization of chemical reactions with reactant ions. This information also advances the study of atmospheric pressure ion kinetics under continuous ionization, which has a role in developing trace level chemical analyzers. In this study, an ionization chamber is described to measure the abundance of ions produced by a 4.9 keV, model L12535, soft x-ray source from Hamamatsu Corporation. Ions of positive and negative polarity were measured independently in an $8 \times 30\,mm^2$ cross section at distances of 12–136 mm at ambient air from an uncollimated beam. Ions were collected using electric fields and 16 sets of plates. The ion current decreased exponentially with distance from the source, and the calculated ion concentration varied between 1.0×10^8 and $3.8 \times 10^5 ions\,cm^{-3}$ on plates. A 2D-COMSOL model including losses by recombination and diffusion was favorably matched to changes in ion current intensity in the ionization chamber. Although the ionization chamber was built to characterize a commercial ion source, the design may be considered generally applicable to other x-ray sources.

I. INTRODUCTION

The ionization of gases with the formation of ions of positive and negative polarity has been a subject of study since the discovery of x rays. Thomson[1] in 1896 studied the so called Röntgenized gas and showed that x rays exhibited a capability to make air conductive between two plates and that the current measured from a charged plate would increase to saturation when the potential between the plates was increased. Rutherford[2] in 1897 studied the conductivity of gases exposed to x rays and demonstrated the nature of the recombination of ions and with an exponential decrease in decay of ions. The ion intensity generated by x rays between 20 and 100 kV was used to determine the x-ray dose rate by Ritz[3] in 1959. More recently, Inaba *et al.*[4] used soft x rays to neutralize static electricity and studied neutralization as a function of distance from a 9.5 kV x-ray source. The amount of charge available from a 9.4 keV soft x-ray source was described by Han *et al.*[5] for unipolar charged nanosized aerosol particles. The rate of ion production was greater than $2.9 \times 10^9\ ions\,cm^{-3}\,s^{-1}$ for both positive and negative ions, and ion densities ranged from 2.5×10^7 to $3.4 \times 10^7 ions\,cm^{-3}$ as a function of electric field used to collect ions.

Soft x-ray ion sources have been included recently in chemical instrumentation where measurements are based on gaseous ions and reactions through atmospheric pressure chemical ionization

(APCI). Döring[6] filed a patent of the non-radioactive ion source for an ion mobility spectrometer (IMS) in 1999. Pershenkov *et al.*[7] installed a 4 keV x-ray tube as the ionization source for a drift time ion mobility spectrometer (DT-IMS) and determined the change in reactant ion current as a function of distance from the x-ray window where the reactant ion current increased with distance from the x-ray source. Reinecke *et al.*[8] replaced a tritium-based ion source with a commercial x-ray source also with an ion mobility spectrometer and evaluated the signal intensity as a function of activity of the x-ray source. Soft x rays between 2.25 and 5 keV were demonstrated with an alternate ion mobility design, the differential ion mobility spectrometer, by Kuklya *et al.*,[9] and ion production was found identical to the widely distributed ion source for IMS, a beta emitter ^{63}Ni. Other applications with x-ray sources were given by Bunert *et al.*,[10] who used a 4.9 keV x-ray source with an orthogonal installation to avoid secondary consequences of x-ray penetration into the inner volume of the drift tube, and Ahrens *et al.*,[11] who used 3 keV x rays as an alternative for tritium in a miniature IMS drift tube. A design with two 4.9 keV x-ray sources in a tandem arrangement permitted fast switching between multiple reagents in atmospheric pressure chemical ionization mass spectrometry by Rissanen *et al.*[12] Riebe *et al.*[13] used 2.8 keV soft x rays as the APCI ionization source for research of photoionization of explosives and dopants. A miniature x-ray source was used instead of the standard APCI source of the ion trap MS also by Erler *et al.*[14] to measure mold fungi.

Despite the significant use of soft x rays in analytical instrumentation, quantitatively little is available in the open literature concerning ion density in air as a function of distance from the source from a soft x-ray source and in a volume where ions are confined in an electric field.

In this report, an ionization chamber is described to allow ion density to be measured in a volume with a confining electric field designed around the cross section of a commercial x-ray source. Ion density in the ionization chamber in an ambient pressure is shown from 12 to 136 mm with a commercial off the shelf (COTS) x-ray source, Hamamatsu L12535. Main advantages of this source are the regulation free 4.9 keV acceleration voltage, small form factor, 24 V input, and low 4 W power requirement. Finally, the design of the ionization chamber was supported by the simulation of electric fields and ion motion in the ionization chamber; in addition, the results of ion formation were compared to the model that simulates x-ray penetration with distance.

II. EXPERIMENTAL

A. Experiment hardware

An ionization chamber built to collect quantitative information of x-ray ionization efficiency (ionization chamber) is shown in Fig. 1. The Hamamatsu L12535 4.9 keV uncollimated ionization source with 120° beam angle [labeled (A)] is located in a 3D printed polylactic acid (PLA) box at left in Fig. 1. Two printed circuit boards (PCBs) with two layers (top and bottom) and green solder mask coverage are joined with six bolts and support rails (polylactic acid) separated by 8 mm. The support rails can be seen in a side view of the ionization chamber as shown in the Appendix in Fig. 8. The mechanical connection between x-ray support, rails, and PCBs is made using hot glue on the outer surface of the PCB and x-ray support.

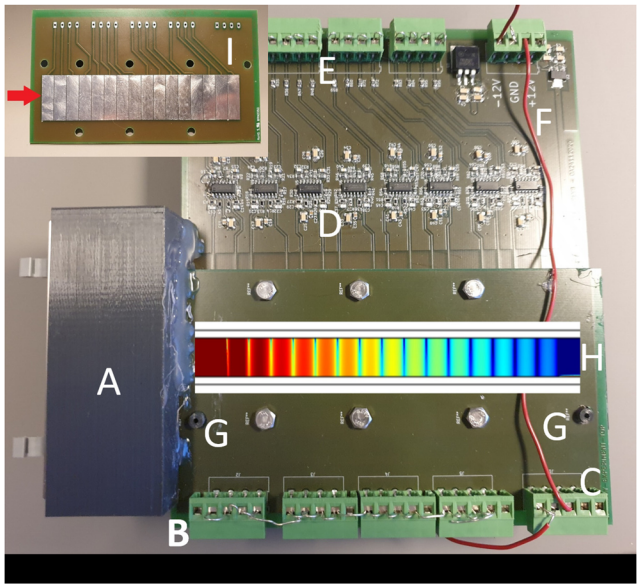

FIG. 1. Ionization chamber constructed from two stacked printed circuit boards (PCBs) to measure the ion yield as a function of distance. A: x-ray source located in 3D printed housing, B: connectors for plates on the top PCB, C: grounding terminal, D: two stage transimpedance amplifiers wired to plates on the bottom PCB, E: terminals connected to amplifiers, F: linear voltage regulators for the amplifiers, G: gas inlet and outlet, not used in this experiment, H: visualization of COMSOL simulated ion concentrations between PCBs, and I: top PCB of the ionization chamber from the plate side. Red arrow indicates the direction of the x rays. Plates are of 8 × 30 mm^2 cross section and separated by 0.25 mm.

The facing surfaces of the PCBs contain 16 metal plates of 8 × 30 mm^2 cross section separated by 0.25 mm (I).

The x-ray window of the Hamamatsu source is placed toward the ionization chamber. The direction of the radiation is shown with a red arrow in the inset of Fig. 1. The distance of the x-ray window is 7 mm from the PCB edge and 12 mm to the middle of the first plate, and the total length of the chamber is 140 mm, while the distance of the last plate is 136 mm.

Plates on the top layer of PCB plates are connected to the screw terminals denoted with letter B and the plates on the bottom layer plates are connected to a two stage transimpedance amplifier chain (D) realized with surface mounted components. The amplifier schematics are given in the Appendix in Fig. 6. The outputs of the second stage of the amplifiers are connected to the screw terminals in the top (E). The first stage of the amplifier has a gain of -10^9 V A^{-1}, while the second stage has a gain of -10 V V^{-1} resulting to the total gain of 10^{10} V A^{-1}. The amplifiers are powered with ±5 V linear regulators (F). The outer surfaces of the PCBs not used for electrical connections are covered with the metal and connected to the ground potential to form a shield against the external electric fields. The ground potentials of top and bottom PCBs are connected together with the wire (C–F) shown in the right of the photo. The wire (C–B) in the near bottom connects the x-ray housing to the ground potential. Two round gray programmable logic array parts (G) are gas connectors and were not used in this work. An embedded bar (H) overlaid on the top of the top PCB is an illustration of the simulated ion concentration between facing top and bottom plates

TABLE I. Parameters for the ionization chamber.

Plate width	30 mm
Plate length	8 mm
Plate spacing	0.25 mm
Plate thickness on the substrate	35 μm
Number of plates	16
Air gap between plates	8 mm
X-ray distance to the middle of the first plate	12 mm
Maximum length of the radiating path	140 mm
X-ray source	4.9 keV, L12535 by Hamamatsu
X-ray photon energy	2–4.9 keV
Amplifier DC gain	10^{10} V A^{-1}
Amplifier output swing	±5 V
PCB thickness	1 mm

under the simulated ionization and applied electric field demonstrating the principle of the operation. Ionization chamber parameters are presented in Table I.

B. Simulation model

The two dimensional, cross-sectional simulation model was built with COMSOL Multiphysics 5.5, Comsol Inc., Burlington, USA. The dimensions of the model are given in Table II. The model incorporates COMSOL's Laminar Flow (spf), Electrostatics (es), Transport of Diluted Species (tds), and Chemistry (chem) physics. Laminar flow and electrostatics were solved as stationary. Transport of Diluted Species and Chemistry were solved time dependent using Laminar Flow and Electrostatics solutions as independent variables for Transported of Diluted Species and Chemistry. Time dependent solutions were solved for 5 s in order to ensure steady state solution. All simulations were solved assuming a temperature of 293 K and 101.3 kPa standard pressure.

The geometry for the simulation has the dimensions of the cross section of the ionization chamber, and it uses air as the material between the top and bottom layers. The PCB material was FR4 in the simulation. The plates are modeled as planar boundaries directly on the surfaces to avoid unnecessary meshing and extra computational load. The top plane top boundary and the top plates are connected to potential U_b to avoid numerical issues in the es simulation. The outmost boundary of the bottom plane with the bottom plates is connected to the ground potential. The mesh used in the simulation was generated based on the used physics, and no manual optimization was done.

TABLE II. Parameters for models using COMSOL.

Plate width	30 mm
Plate length	8 mm
Plate spacing	0.25 mm
Air gap between plates	8 mm
Recombination coefficient of RP and RN	1×10^{-6} cm^3 s^{-1}
Mobility of RP and RN	2.1 cm^2 V^{-1} s^{-1}
Signal intensity modification gain a	0.0585

For the Transport of Diluted Species simulation, both positive and negative ions were introduced. The transportation of the ions was simulated with electric mobility and a fluid flow. The electric mobility of ions was introduced via diffusion. The diffusion constant (m^2 s^{-1}) was derived from electrical mobility with the following equation:

$$D = k_0 \frac{T k_B}{q_0}, \tag{1}$$

where k_0 is the ion's mobility, here assumed as 2.1 cm^2 V^{-1} s^{-1}, T is temperature K, k_B is the Boltzmann constant (1.38×10^{-23} kg m^2 K^{-1} s^{-2}), and q_0 is the elementary charge ($1.602 \times 10^{-19} C$). The positive ions were introduced with the charge parameter $Z = 1$ and negative ions with parameter $Z = -1$. The charge density was considered so low so the impact to the electric field or interactions based on electrostatic forces between positive and negative ions could be neglected.

The concentration of the ions was solved with Transport of Dilutes Species combined with Chemistry physics. Ions were introduced into the air gap with constant rate using the reaction node in Transport of Diluted Species physics, simulating the constant ionization caused by the x-ray source. The production rate was estimated with a function that models the geometry and the decay of x rays in air. The model parameters were obtained from the measured data, and it is assumed that the ion current equals to the production of ions in the volume over the plates. The formula used to fit the COMSOL model with measurement data is

$$\frac{i(x)}{q_0 N_A V_{CH}} = a I_0 \frac{h}{h - 1.732x} e^{-\beta x}. \tag{2}$$

The left-hand side of Eq. (2) describes the amount of ions created in the volume of air over the plates, and the right side is a model used in COMSOL. The term $h/(h - 1.732x)$ in the COMSOL part approximates the intensity loss of the uncollimated beam that exits the x-ray source in 120° and enters to square shaped chamber. The term $e^{-\beta x}$ describes the loss of beam intensity due the absorption in the air. The parameters are as follows: $i(x)$ is the measured ion current (A), q_0 is the elementary charge (C), N_A is the Avogadro number (6.022×10^{23} mol^{-1}), V_{CH} is the volume over the plate (1.92 cm^3), a is the fitting multiplier for the intensity, I_0 is the intensity obtained from the measured data (mol s^{-1} m^{-3}), h is the height of the ionization chamber (8 mm), β is the decay parameter (m^{-1}), and x is the distance from the source. The parameter a is used to scale real life 3D data to 2D simulation. It should be noted that the parameter a was found iteratively and was initially selected as 1 in simulation.

Positive and negative ions are named in the COMSOL simulation model as R^+ and R^- and were introduced into the simulation domain equally. The diffusion was included into the model via electric mobility with Eq. (1). The recombination of R^+ and R^- was introduced as a reaction [Eq. (3)] resulting to virtual species R with no charge and interaction to other components and thus no transfer properties. The recombination reaction rate used was 1×10^{-6} cm^3 s^{-1} (see the work of Siegel[15]). The time dependent solver was used, and all solutions were solved between 0 and 5 s. The ions in the simulation model were transported to the plates by an electric field. The current on the plate was calculated as an integral

of the ion flux via the plate multiplied by the elementary charge,

$$R^+ + R^- \rightarrow 2R. \quad (3)$$

C. Measurement setup

A cardboard box covered with aluminum tape and foil was used to shield the ionization chamber against 50 Hz interference and other external electrical noise during the measurements. The box was grounded to the DC power supply ground terminal that was connected to the measurement ground too. Amplifiers were powered from two serially connected 9 V batteries via +5 and −5 V linear regulators embedded on the bottom board. The battery stack midpoint potential was connected to the DC ground. The x-ray source was powered from the L12535 controller model C12537 from Hamamatsu. The electric potential U_b was generated by the DC power supply EA-PS 2342-06B from Electro Automatic GmBH, Germany, and was connected to the screw terminals of the top PCB. The current signal was recorded one by one from the bottom PCB screw terminal with PicoScope 6-PC, v. 6.14.13.5207 software using PicoSope 2206B from Pico Technology Ltd. UK, using 1× probe, 20 s sample interval for 1 s and stored data to the file in the ASCII (American Standard Code for Information Interchange, character encoding) format resulting to 5000 samples each. The x-ray source was turned off when the scope probe was moved between the screw terminals and turned on again before next measurement. A healthy check for all amplifiers was performed before the sequence for the x-ray experiment was run. The offset and the noise level of each amplifier were recorded showing < 6 and < 1 mV standard deviation noise, respectively, for all 16 amplifiers. Positive ion data were recorded with an U_b of 0, 2, 5, 10, 15, 25, 30, 35, and 40 V, 0 V for housekeeping purposes only. Measurements were repeated five times for each setting during the four day period. Negative ion data were measured once for U_b −2, −5, −10, and −40 V after the last repetition of the positive ion collection sequence.

The gain of the two stage amplifier was 10^{10} V A^{-1}, and the maximum output swing of the amplifiers was ±5 V, corresponding to ±500pA as that measured current that limits the detectable current. However, the gain of the first amplifier in the chain was 10^9 V A^{-1}, which allowed detecting the larger current input although the ionization chamber was not designed for this. The current signal from the first four plates was measured once directly from the output of the first amplifier with U_b 5, 10, 35, and 40 V. It should be noted that due to the electric field direction between plates, the positive ions were collected when U_b was positive and negative ones were collected when U_b was negative.

All measurements were done in room temperature of about 296 K (23 °C) with ambient air in the air gap. The humidity was uncontrolled, but relative humidity was measured to be 39% during the first measurement day. The pressure was not controlled, and the ambient pressure varied between 991 and 1008 mbar during the four day measurement period. Humidity and pressure were recorded with an uncalibrated barometer for reference only.

D. Data processing

The data were loaded to RStudio, V 1.2.5033 from RStudio Inc (R). The data from each channel and U_b were loaded, converted to amperes using the gain of the amplifiers, and averaged, and the average of the corresponding offset signal (U_b = 0) was subtracted. No other filtering for the data was performed. The current signals were converted to ion concentration using the following equation:

$$c(x) = \frac{i(x)}{q_0 k_0 \frac{U_b}{h} WL}, \quad (4)$$

where $c(x)$ is the density (cm^{-3}), $i(x)$ is the measured current (A), q_0 is the elementary charge (C), k_0 is the assumed average mobility of ions (cm^2 V^{-1} s^{-1}), U_b is the voltage (V) set between measurement plates, h is the height of the measurement chamber (8 mm), W is the width of the plate (30 mm), and L is the length of the plate (8 mm). The measured current signal was fitted to the mathematical model using equation Eq. (5) using function nls in software R. The parameter notation in Eq. (5) equals to Eq. (2),

$$i(x) = I_0 \frac{h}{h - 1.732x} e^{-\beta x}. \quad (5)$$

The measured current signal was fitted to the COMSOL model given in Eq. (2) using the function nls in software R separately for each tested electric field, and the obtained I_0 and β parameters were applied via the interpolation function in COMSOL simulation. Data were plotted using R's built in plot function and some R scripting.

III. RESULTS AND DISCUSSION

The current from the ions produced by the Hamamatsu x-ray source, in air at ambient pressure, is shown in Fig. 2 for each of the 16 plates in the ionization chamber (Fig. 1, inset). The amplifier gain for each plate was 10^{10} V A^{-1} (solid lines) from 45 to 136 mm and 10^9 V A^{-1} (dotted lines) for first four plates placed from 12 to 37 mm.

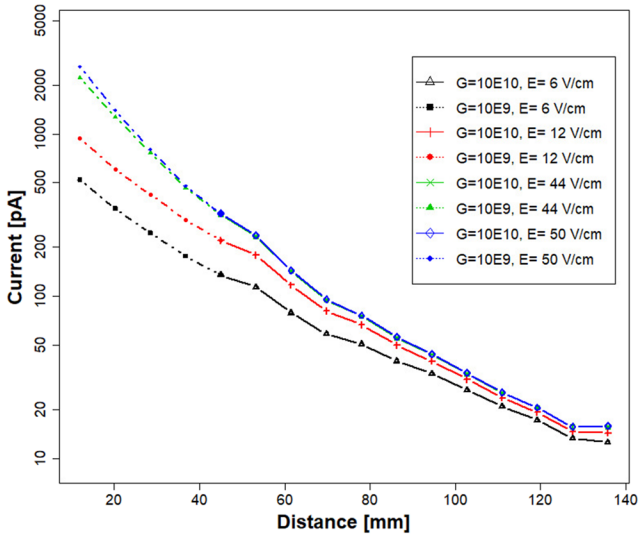

FIG. 2. Positive ions measured with a gain of 10^9 V A^{-1} from plates placed in the distances between 12 and 37 mm combined with the result measured with a gain of 10^{10} V A^{-1} in distances between 45 and 136 mm. The maximum current at a distance of 12 mm was 2.59 nA when the electric field was 50 V cm^{-1}.

The distances from the x-ray source were measured at the center of each plate, and a uniform electric field (E) between plates could be established from 2 to 50 V cm^{-1} since plates on the top plane of the chamber could be floated to certain positive or negative DC potentials (U_b) and plates connected to amplifiers were connected to virtual ground. The plots in Fig. 2 are shown for positive ions, collected at top plates with a positive bias, and negative ions (not shown) were collected at top plates with a negative bias. While plots were obtained at 20 steps of field strength, only four are shown in this figure to illustrate the dependence of the intensity of current on E. Figure 3 is the same, but for both positive and negative ions with an amplifier gain of 10^{10} V A^{-1} for each plate. Semilog plots in Figs. 2 and 3, show that the current intensity increases proportional to E. In Fig. 3, a plateau in response is reached when approaching 50 V cm^{-1} when the distance is less than 37 mm and the field strength is increased. This is because of the amplifier saturation when the gain was 10^{10} V A^{-1}. Identical findings were obtained for negative ions.

The plots in Fig. 2 exhibited a proportional decrease in current as a function of the distance, and this is associated with the formation of gas ions throughout the length of the ionization chamber, that is, the extent of penetration of soft x rays into air at ambient pressure. The findings are also consistent with the existing understandings on the exponential decay of ionization efficiency with distance from x-ray sources. The near equal response between plates at distances of 128 and 136 mm are attributed to fringe fields and distortions in E at the end of the ionization chamber. A systematic deviation seen in all curves in plots of Figs. 2 and 3 (as log-linear format) was associated with commercial tolerances for manufacture of individual amplifiers and associated components (see Appendix, Fig. 6).

Comparisons can be made in Fig. 3 as semi-log plots of current on plates for negative ions (dotted lines) and positive ions (solid lines) for selected values of E including ±2, ±6, ±12, and ±50 V cm^{-1} with an amplifier gain of 10^{10} V A^{-1}. The alignment of plots for positive and negative ions demonstrates that ion currents from each polarity are identical within experimental error, and this is consistent with charge balance for ion pairs formed by x-ray ionization. Although ion identities were not determined in this study, hydrated protons $H^+(H_2O)_n$ and oxygen anions $O_2^-(H_2O)_n$ are known to form at ambient pressure in a purified air atmosphere (see the work of Borsdorf and Eiceman[16]). Since the composition of air in these studies were not rigorously purified, the ions in these measurements (with FR4 PCB planes) are likely adduct derivatives such as $MH^+(H_2O)_x$ and $MO_2^-(H_2O)_y$, where M can be a selection of volatile organic compounds found as complex mixtures as airborne vapors in indoor atmospheres or constituents of circuit boards released into the headspace of the ionization chamber.

A detailed measure of the efficiency of ion collection with the strength of the electric field between plates is shown in Fig. 4 as plots of current (with 3 standard deviation error bars) vs distance. The current reaches a plateau in response at each distance as the electric field increases. At this condition, ion production has reached a steady state with loss mechanisms including diffusion, recombination, and collection efficiency. At the closest distance from the x-ray source, the ion production is high and a high field is necessary for reaching the plateau, and where the ion yield is low, the plateau is reached with smaller field strength. At the low field values, diffusion and recombination dominate as the transportation of ions to the plates is slow with significant time for such losses. When the field strength is increased, residence times of ions in transit to plates will decrease. Consequently, diffusion and recombination losses will

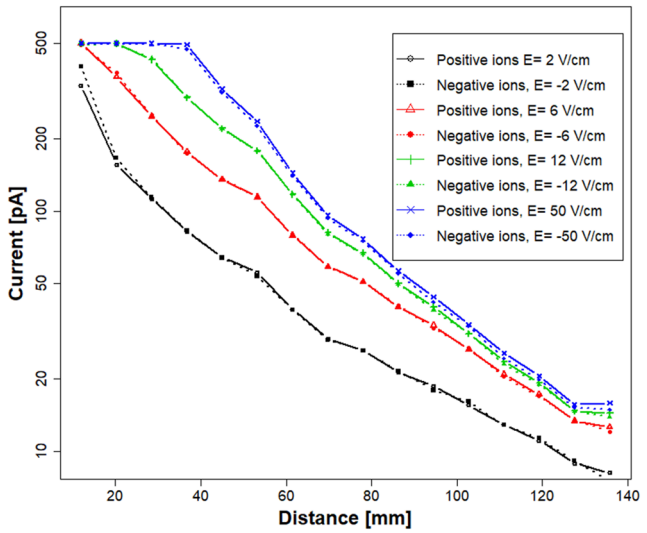

FIG. 3. Current from positive and negative ions with selected field settings. Both polarities are measured with an amplifier gain of 10^{10} V A^{-1}, which limits the maximum measurable current to 500 pA.

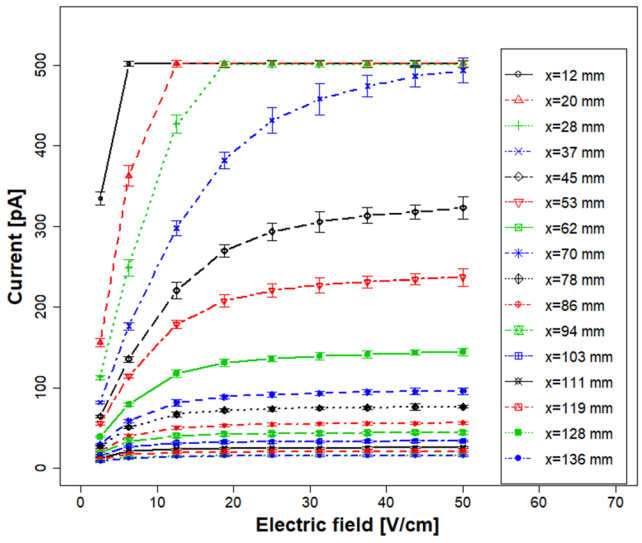

FIG. 4. Positive ion current presented as a function of electric field for various distances. 3 standard deviation error bars are shown over the measured values. Current saturates when the field is increased because the number of ions created by x rays meets the loss mechanisms including ion removal by the electric field, recombination, and diffusion loss. Due to the exponential loss of ionization capacity, the ion current is small compared to closer plates when the distance exceeds 86 mm.

decrease too and current values may be considered the maximum availability of ions produced by the soft x-ray ion source available for later uses in chemical measurements using atmospheric pressure chemical ionization reactions.

The magnitude of current on a plate corresponds to the rate of ion collection through electric field mobility,

$$v_d = k_0 E, \tag{6}$$

where v_d is the velocity of drift of ions as swarms ($\mathrm{cm\,s^{-1}}$), k_0 is the mobility coefficient ($\mathrm{cm^2\,V^{-1}\,s^{-1}}$), and E is the electric field ($\mathrm{V\,cm^{-1}}$). The efficiency of ion capture should increase with E as diffusion losses and recombination are reduced with decreased residence time of ions in the gap. The value for k_0 is estimated here as $2.1\,\mathrm{cm^2\,V^{-1}\,s^{-1}}$, and the values for v_d are calculated [Eq. (6)] as 4.2–105 $\mathrm{cm\,s^{-1}}$. Since the ions are generated continuously by the x-ray source, the current measured arises from the ion flux between the plates. Thus, the maximum residence time of ions between plates occurs for ions generated near the surface of the opposing plate. These ions must move through the entire gap between plates. These assumptions permit ion residence times could be estimated as 190 ms at $2\,\mathrm{V\,cm^{-1}}$ to 7.6 ms at $50\,\mathrm{V\,cm^{-1}}$.

Values for the density of ions derived from the current intensity [see Eq. (4)] are given in Table III. The highest density of $1.00 \times 10^8\,\mathrm{cm^{-3}}$ was found at 12 mm with $6\,\mathrm{V\,cm^{-1}}$ electric field, but it should be noted that the obtained value depends on the selected k_0. As explained before, the ions are a mixture of unknown result ions and thus a mixture of various values of k_0. The value of k_0 can vary between 0.5 and $3\,\mathrm{cm^2\,V\,s^{-1}}$, and therefore, the uncertainty is in order of four. The density of ions measured instantaneously decreases with increased E and, though counterintuitive perhaps, is a consequence of the rapid removal of ions with increased electric field strength.

The match between experimental measurements and a mathematical model shown in Eq. (5) is given in Fig. 5 for plots of

TABLE III. Ion density $\mathrm{cm^{-3}}$ as a function of distance.

mm	6 ($\mathrm{V\,cm^{-1}}$)	12 ($\mathrm{V\,cm^{-1}}$)	44 ($\mathrm{V\,cm^{-1}}$)	50 ($\mathrm{V\,cm^{-1}}$)
12	1.00×10^8	9.05×10^7	6.07×10^7	6.23×10^7
20	6.65×10^7	5.80×10^7	3.47×10^7	3.36×10^7
28	4.71×10^7	4.06×10^7	2.10×10^7	1.92×10^7
37	3.39×10^7	2.83×10^7	1.27×10^7	1.15×10^7
45	2.60×10^7	2.12×10^7	8.72×10^6	7.75×10^6
53	2.20×10^7	1.72×10^7	6.43×10^6	5.68×10^6
62	1.52×10^7	1.13×10^7	3.93×10^6	3.46×10^6
70	1.13×10^7	7.80×10^6	2.61×10^6	2.30×10^6
78	9.78×10^6	6.42×10^6	2.08×10^6	1.83×10^6
86	7.67×10^6	4.81×10^6	1.53×10^6	1.35×10^6
94	6.41×10^6	3.83×10^6	1.20×10^6	1.06×10^6
103	5.10×10^6	2.97×10^6	9.17×10^5	8.08×10^5
111	4.01×10^6	2.27×10^6	6.98×10^5	6.15×10^5
119	3.31×10^6	1.85×10^6	5.66×10^5	4.95×10^5
128	2.57×10^6	1.41×10^6	4.31×10^5	3.76×10^5
136	2.42×10^6	1.38×10^6	4.31×10^5	3.81×10^5

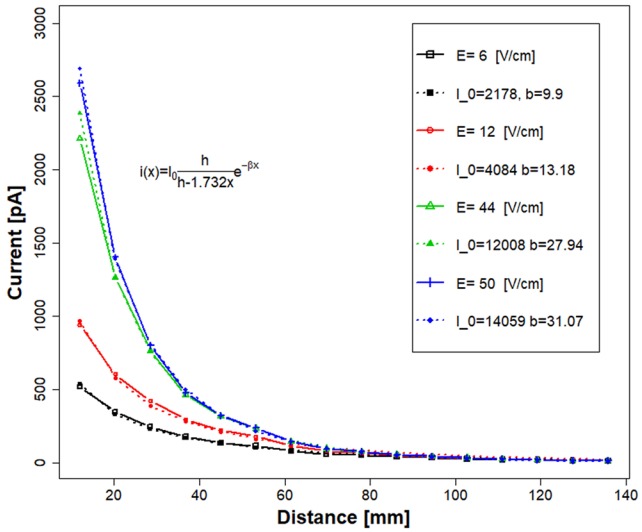

FIG. 5. Data shown in Fig. 2 (solid lines) compared to predicted current (dotted lines) by the fitted model for selected fields. The model overestimates the current for short distances and high field. Parameters h and x are in meters and I_0 is in pA. The solid labels show the electric field, and the dotted labels show the estimated parameter values. Note that I_0 and b in the label equals I_0 and β correspondingly in Eq. (5), which is also shown in the plot.

the measured current intensity (solid lines) and distance from the x-ray source. The plots with dotted lines are shown for the values estimated using the model and only in few samples for the electric field ($6, 12, 44, 50\,\mathrm{V\,cm^{-1}}$), which are shown for clarity. When terms are $E = 50\,\mathrm{V\,cm^{-1}}$, $I_0 = 14 \times 10^3$ pA, and $\beta = 31\,\mathrm{m^{-1}}$, the estimated data at the low field match the measured current, but in the high field and close distance, the estimates are higher than the measured values. The discretization of distance in measured data is not optimal for fitting because the rate of change in the close extent of the x-ray window is high, but plates are equally spaced and wide compared to the rate of the change. Another reason may be that the approximation used to describe the collimation effect near the x-ray window is insufficient, leading to overshoot in the fitting.

Models for simulation of ion production and detection were made using COMSOL with electric field (E) values of 6, 12, 44, and $50\,\mathrm{V\,cm^{-1}}$. The measured data and simulated results are compared in Table IV. When simulated with $6\,\mathrm{V\,cm^{-1}}$, the model predicts smaller values than the measured data, while simulating with 44 or $50\,\mathrm{V\,cm^{-1}}$ results in higher values than measured. The best fit was found with $12\,\mathrm{V\,cm^{-1}}$.

TABLE IV. Mean and rms error between the measured ion current and COMSOL simulated ion current for selected electric field values for plates 2–16. The best fit was for $12\,\mathrm{V\,cm^{-1}}$.

	6 ($\mathrm{V\,cm^{-1}}$)	12 ($\mathrm{V\,cm^{-1}}$)	44 ($\mathrm{V\,cm^{-1}}$)	50 ($\mathrm{V\,cm^{-1}}$)
Mean error (%)	27.6	9.00	−11.4	−15.8
rms error (%)	28.2	13.6	20.5	24.0

The deviations between the COMSOL simulation model results and measured data can be described by the differences between the ionization chamber and certain parameters chosen to simplify simulations. For example, the x-ray window and the surrounding metal case in the ionization chamber are grounded in practice though not in the simulation entrance. In addition, the first 7 mm in the ionization chamber is an ungrounded surface, so the stray field can force ions toward the x-ray source. In the simulation model, ions generated between 0 and 7 mm sum up with ions generated over the plate, and thus, the first simulated value overshoots. These arrangements or choices for the simulation model were necessary to ensure the numerical stability and simulation convergence. While such differences are not likely to contribute significantly to discrepancies, a detailed quantitative analysis of this is beyond the scope of this present work. Finally, the decay model is an approximation, and while some inaccuracies exist between the model and measured data, the simulation model serves as a platform for future steps, particularly when refined.

IV. CONCLUSION

An ionization chamber to measure atmospheric ion concentration distribution as a function of distance from the 4.9 keV uncollimated x-ray source was built to find parameters for the theoretical study of kinetics. Data were recorded at distances between 12 and 136 mm. Both positive and negative ions were measured. The ion concentration distribution was found to follow exponential decay, and it was equal for both positive and negative ions. The maximum ion concentration was 1.0×10^8 cm^{-3} at 12 mm and dropped over two decades to 3.8×10^5 cm^{-3} at 136 mm. A 2D model to simulate the ionization chamber was created, and the simulation parameters were obtained from the ionization chamber and measured data. The simulation model needs further improvement, but already as is it can be used for further experiment development.

AUTHORS' CONTRIBUTIONS

O.A. contributed to test apparatus design and construction, data collection, graphs, and simulation and O.A., E.L., T.K., and G.E. helped in data interpretation and manuscript preparation. All authors reviewed the results and approved the final version of the manuscript.

ACKNOWLEDGMENTS

The authors would like to thank the following people: Dr. George Pallis from T4i engineering, UK, for help with rail manufacture for the ionization chamber fabrication; Karsa Oy, Finland, for the loan of a PhotoIonBar power supply; and Bert Ungethüm from Airsense Analytics GmbH, Germany, for COMSOL simulation tips. This project has received funding from the European Union's Horizon 2020 FET Open program under Grant Agreement No. 899261.

APPENDIX: ELECTRONICS, DATA, AND COMSOL SIMULATION

1. Ionization chamber electronics

The ion current in the ionization chamber-apparatus was measured with a two stage amplifier realized with LMC6484 operational amplifiers. The first stage has a DC gain of -1×10^9 V A^{-1}, and the second stage has a DC gain of -10 V V^{-1}, so the overall DC gain is 1×10^{10} V A^{-1}. To minimize the inductive noise pickup, the amplifiers were realized with surface mounted components. The input of the amplifier is connected to the virtual ground of the first operational amplifier, and an external electric field is used to drive ions to the measurement plate. The schematic and PCB design was done with KiCad, V 5.1.7-1. The schematic of the amplifier is shown in Fig. 6. The bottom PCB layout is shown in Fig. 7, and construction of the apparatus is shown in Fig. 8.

2. Storing of experimental data

Experimental data were stored in the ASCII text files and are available on request from the corresponding author in a packed format (GID-X-RAY-DATA.ZIP). The data are stored in several folders with the following names:

- M1601, M1701a, M1701b, M1801a, M1901: positive ions, measured between 0 and 40 V;
- M2301: negative ions, measured between 2 and 40 V; and
- M2801: positive ions, extended range, measured only for few channels and voltages.

The files have the following systematic naming convention:

- GIX-Vxx (i).txt: positive ions, xx used collection voltage in volts; i denotes the amplifier, i = 1 means CH1, 12 mm from the source, and i = 16 means CH16, 136 mm from the source;
- GIN-Vxx (i).txt: negative ions, xx used collection voltage in volts; i denotes the amplifier, i = 1 means CH1, 12 mm from the source, and i = 16 means CH16, 136 mm from the source; and
- GIXN-Vxx (i).txt: positive ions measured from the output of first amplifier, therefore negative sign.

It should be noted that the data in the files are expressed either in volts or in millivolts depending on the setting used during the collection phase. The scope range settings were adjusted to proper range during data collection. The range setting is present in the title lines of the data files.

The data are available from the corresponding author on request.

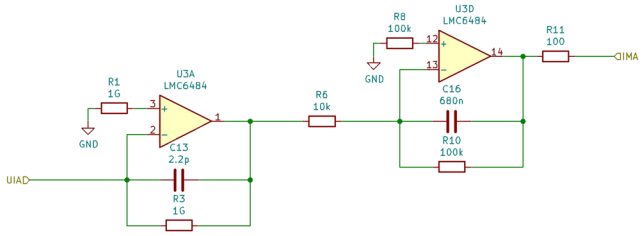

FIG. 6. Two stage transimpedance amplifier used to convert current to voltage in the ionization chamber. The first stage has a gain of -10^9 V A^{-1}, and the second stage has a gain of -10 V V^{-1}. R11, 100R resistor, is used to protect the second amplifier output from short circuit.

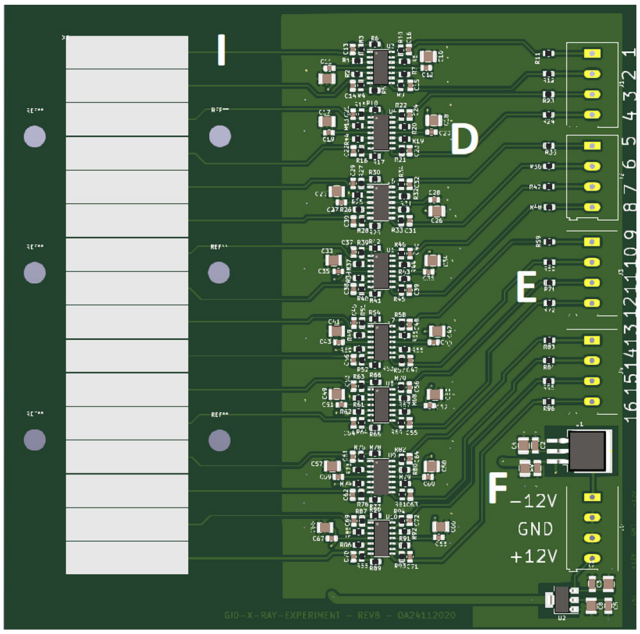

FIG. 7. Ionization chamber layout design of the bottom PCB printed from KiCad 3D-viewer. I: connected to amplifiers, D: amplifiers, E: terminals for measurement, and F: linear voltage regulators for amplifiers.

3. COMSOL model

The COMSOL model (GID-X-RAY-model-Supplementary.mph) is available as is from the corresponding author on request. The model has been built with COMSOL 5.5. The model has the following four studies:

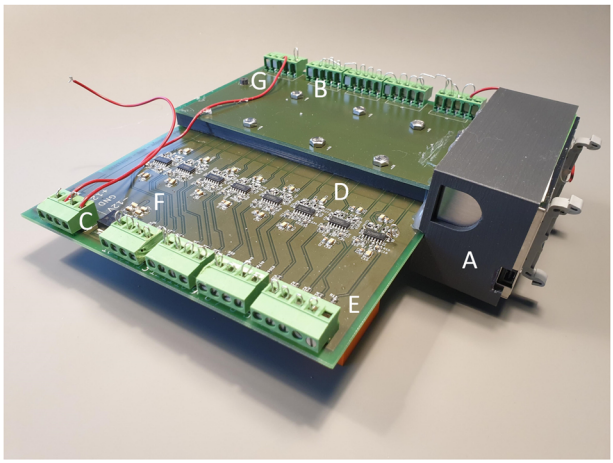

FIG. 8. Mounted ionization chamber showing the separating rail between top and bottom PCBs and the x-ray source holder. A: x-ray source located in 3D printed housing, B: connectors for plates on the top PCB, C: grounding terminal, D: two stage transimpedance amplifiers wired to plates on the bottom PCB, E: terminals connected to amplifiers, F: linear voltage regulators for the amplifiers, and G: gas inlet and outlet, not used in this experiment.

- Study 1: stationary study of flow and electric field.
- Study 2: time dependent study of transport of diluted species and chemistry.
- Study 3: parametric study to variate potential to create an electric field. This study combines study 1 and study 2.
- Study 4: non-parametric study that combines the stationary study for flow and electric field and the time dependent study for transport of diluted species and chemistry.

Study 2 cannot be run until study 1 is run because values from study 1 are used in the solution for study 2. Study 3 and study 4 can be run as is. In this model, the flow is always zero, but it was built in for future use.

Several parameters have been introduced in the Global Definitions Parameters node. The parameters are used to define the geometry but also to control some settings in the model. Some parameters stored in the parameter table were used during model testing and iteration but are not relevant for the simulation.

The ion production is modeled with a self-written function constconc(x,h,Qfun(U0), betafun(U0)-gamma) [see Eq. (2)]. The shape of this function is shown in Fig. 9, but actual values depend on the parameter values provided by functions Qfun(U0) and betafun(U0) (see Figs. 10 and 11).

Qfun(U0) is an interpolation of the fitting values, which were calculated from measured data as a function of used electric field generation voltage U0. The shape of the function is shown in Fig. 10. Correspondingly, betafun(U0) is a parameter of the exponential part of the fitting, also calculated from the measured data. Data are presented in Fig. 11.

4. Additional simulation results

The electric field norm caused by $U0 = 40$ V at the top plates simulated over 1 mm of the bottom plates is presented in Fig. 12. The field is very smooth, but intentional vertical axis scaling is used to demonstrate the effect of the difference between the field strength over the plates and between them. Figure 13 shows the positive ion

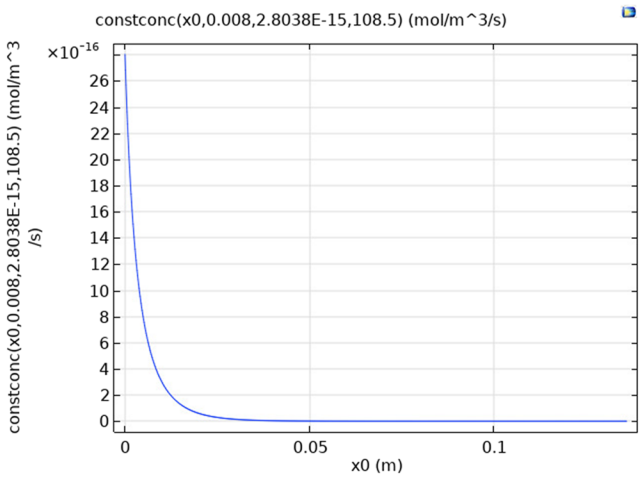

FIG. 9. Prototype of the constconc function used in simulation. The function response is shown with arbitrary parameters.

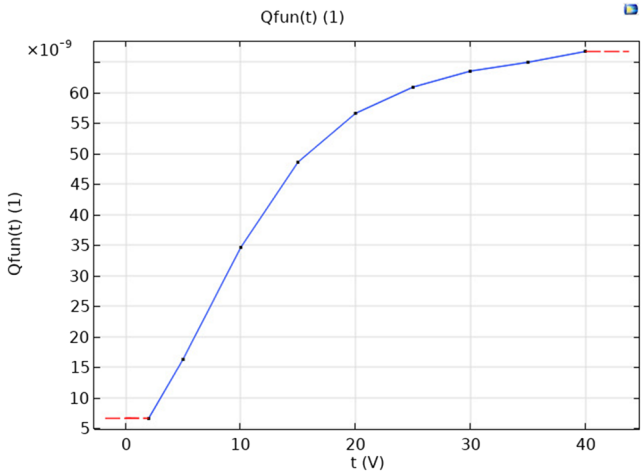

FIG. 10. Interpolation curve of initial intensity I_0 [see Eq. (2)] of the ionization. Values are obtained from experimental data. Note that the prototype parameter t in the figure is replaced with U0 in the simulation.

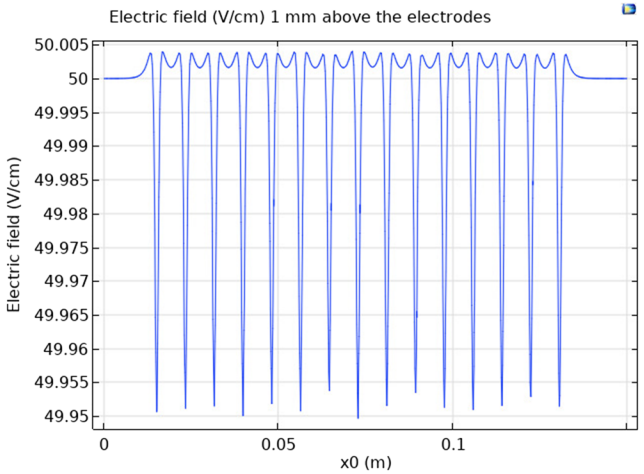

FIG. 12. Simulated electric field 1 mm over the ionization chamber at $U0 = 40$ V. The variation of the field strength is only about 0.1%.

flux toward the plates when simulated up to 5 s. Simulation steps are stored in 1 s intervals, steady state has been reached already during the first two steps, and the subsequent steps cannot be seen separated as they merge in the plot. The field focuses ions toward plates and the flux between the plates is small compared to the peak values.

Simulation included recombination. The recombination was introduced as a simple reaction between positive and negative ions resulting to virtual neutrals, which did not have transportation characteristics or other interactions with positive or negative ions anymore. This method was useful to check that the recombination is truly simulated because the concentration of virtual neutrals was expected to increase over the time. The result of this is seen in Fig. 14. The concentration of the virtual neutrals increases over time although the flux shown in Fig. 13 reaches a steady state.

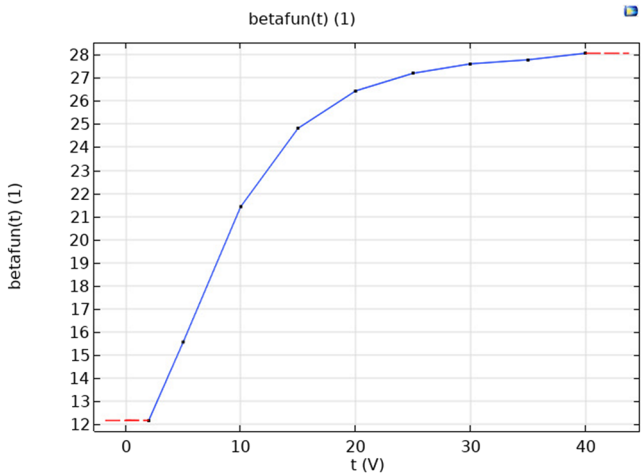

FIG. 11. Interpolation curve of the exponential loss parameter β [see Eq. (2)] of the ionization. Values are obtained from experimental data. Note that the prototype parameter t in the figure is replaced with U0 in the simulation.

a. Few comments about the COMSOL model

The model and the measurements fit quantitatively best only with limited conditions such as the field of 12 V cm^{-1}, but the model underestimates the ion current with low field values and overestimates in high values (Fig. 15). One possible explanation for this is the difference how electric fields are set up in the simulation causing mismatch between the data and simulation at the first channel. Another big difference is that the model is 2D instead of 3D, which brings even more uncertainty to the setup of stray fields and x-ray entrance into the ionization chamber. Unfortunately, using the 3D model is out of our computational resources.

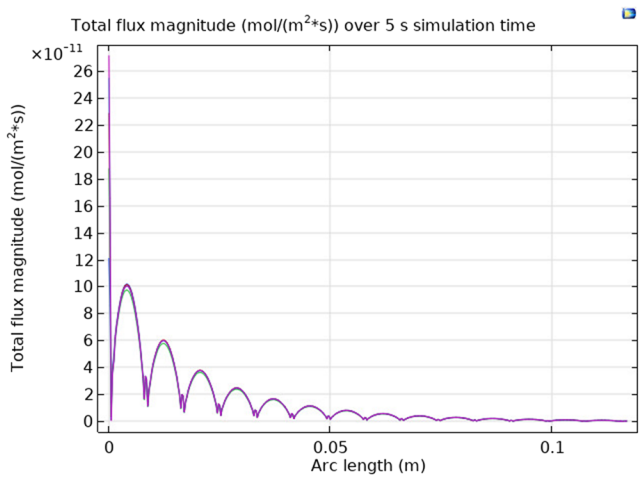

FIG. 13. Positive ion flux toward the measurement plates in the ionization chambers simulated up to 5 s shown with 1 s intervals. Ion current is an integral of the ion flux multiplied by the elementary charge. Steady state has been reached in the first two steps.

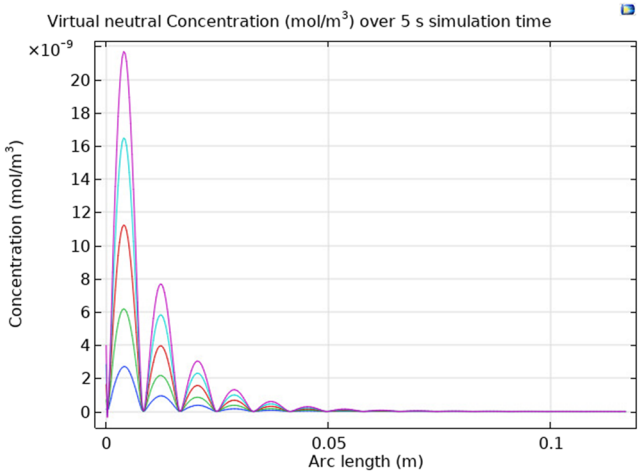

FIG. 14. Virtual neutral ion concentration in the ionization chamber volume as a result of the recombination process when simulated for 5 s shown with 1 s intervals. Different colors represent concentration at stored intervals. Concentration of virtual neutrals increases in every step.

The model is also based on the assumption that all ions are similar with similar electrical mobility or recombination characteristics. This is not true, and in the experimental setup, the quality of ions was not controlled. It is expected, although not verified by any analytical instrument, that the measured current is the result of a complex mixture of ions that behave slightly differently in low and high fields because the available reaction time differs in the air gap depending on the used field.

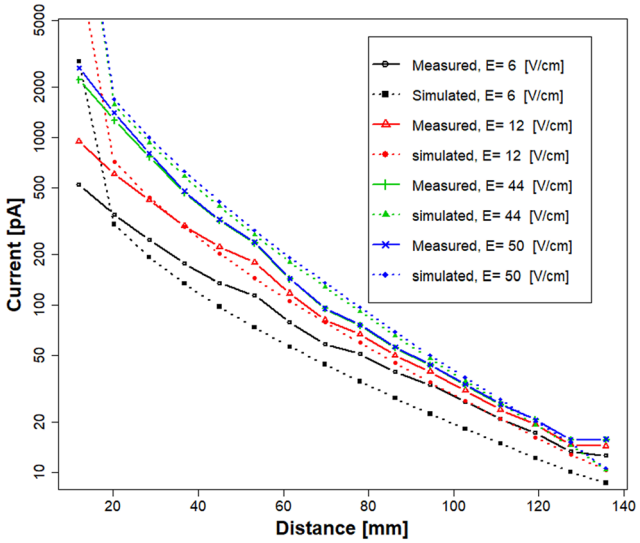

FIG. 15. Experimental data [solid lines, Fig. 2] compared to simulation from COMSOL (dotted lines). The model underestimates the signal when simulating with low field but overestimates the signal when simulated with high field. The simulated current overshoots at the first plate. This is caused by the electric field setup in the COMSOL model to ensure numerical stability. The error between the measured and simulated data is shown in Table IV.

The future steps will include model improvement and work with flow and kinetics. Despite some weakness found in the existing model, it is a fast way to evaluate ideas before investing massively to experimental construction work.

DATA AVAILABILITY

The data that support the findings of this study are available from the corresponding author upon reasonable request.

REFERENCES

[1]J. J. Thomson and E. Rutherford, "XL. On the passage of electricity through gases exposed to Röntgen rays," London, Edinburgh Dublin Philos. Mag. J. Sci. **42**, 392–407 (1896).
[2]E. Rutherford, "LIV. The velocity and rate of recombination of the ions of gases exposed to Röntgen radiation," London, Edinburgh Dublin Philos. Mag. J. Sci. **44**, 422–440 (1987).
[3]V. H. Ritz, "Design of free-air ionization chambers for the soft x-ray region (20–100 kv)," Radiology **73**, 911–922 (1959).
[4]H. Inaba, T. Ohmi, T. Yoshida, and T. Okada, "Neutralization of static electricity by soft X-rays and vacuum UV radiation," J. Electrost. **33**, 15–42 (1994).
[5]B. Han, M. Shimada, M. Choi, and K. Okuyama, "Unipolar charging of nano-sized aerosol particles using soft X-ray photoionization," Aerosol Sci. Technol. **37**, 330–341 (2003).
[6]H.-R. Döring, "Ionisationskammer mit einer nicht-radioaktiven ionisationsquelle," DE19933650, (1999), https://www.freepatentsonline.com/DE19933650C1.html.
[7]V. S. Pershenkov, A. D. Tremasov, V. V. Belyakov, A. U. Razvalyaev, and V. S. Mochkin, "X-ray ion mobility spectrometer," Microelectron. Reliab. **46**, 641–644 (2006).
[8]T. Reinecke, A. T. Kirk, A. Heptner, D. Niebuhr, S. Böttger, and S. Zimmermann, "A compact high-resolution X-ray ion mobility spectrometer," Rev. Sci. Instrum. **87**, 053120 (2016).
[9]A. Kuklya, T. Reinecke, F. Uteschil, K. Kerpen, S. Zimmermann, and U. Telgheder, "X-ray ionization differential ion mobility spectrometry," Talanta **162**, 159–166 (2017).
[10]E. Bunert, T. Reinecke, A. T. Kirk, A. Bohnhorst, and S. Zimmermann, "Ion mobility spectrometer with orthogonal X-ray source for increased sensitivity," Talanta **185**, 537–541 (2018).
[11]A. Ahrens, M. Hitzemann, and S. Zimmermann, "Miniaturized high-performance drift tube ion mobility spectrometer," Int. J. Ion Mobility Spectrom. **22**, 77–83 (2019).
[12]M. P. Rissanen, J. Mikkilä, S. Iyer, and J. Hakala, "Multi-scheme chemical ionization inlet (MION) for fast switching of reagent ion chemistry in atmospheric pressure chemical ionization mass spectrometry (CIMS) applications," Atmos. Meas. Tech. **12**, 6635–6646 (2019).
[13]D. Riebe, A. Erler, T. Ritschel, T. Beitz, H.-G. Löhmannsröben, A. Beil, M. Blaschke, and T. Ludwig, "Atmospheric pressure chemical ionization of explosives induced by soft X-radiation in ion mobility spectrometry: Mass spectrometric investigation of the ionization reactions of drift gasses, dopants and alkyl nitrates," J. Mass Spectrom. **51**, 566–577 (2016).
[14]A. Erler, D. Riebe, T. Beitz, H.-G. Löhmannsröben, D. Grothusheitkamp, T. Kunz, and F.-J. Methner, "Detection of volatile organic compounds in the headspace above mold fungi by GC-soft X-radiation–based APCI-MS," J. Mass Spectrom. **53**, 911–920 (2018).
[15]M. W. Siegel and W. L. Fite, "Terminal ions in weak atmospheric pressure plasmas. Applications of atmospheric pressure ionization to trace impurity analysis in gases," J. Phys. Chem. **80**, 2871–2881 (1976).
[16]H. Borsdorf and G. A. Eiceman, "Ion mobility spectrometry: Principles and applications," Appl. Spectrosc. Rev. **41**, 323–375 (2006).